Sustainable Design-Oriented Level Set Topology Optimization

Jikai Liu[1]
Department of Mechanical Engineering,
University of Alberta,
Edmonton, AB T6G 1H9, Canada
e-mail: jikai@ualberta.ca

Yongsheng Ma
Department of Mechanical Engineering,
University of Alberta,
Edmonton, AB T6G 1H9, Canada

This paper presents a novel sustainable design-oriented level set topology optimization method. It addresses the sustainability issue in product family design, which means an end-of-life (EoL) product can be remanufactured through subtractive machining into another lower-level model within the product family. In this way, the EoL product is recycled in an environmental-friendly and energy-saving manner. Technically, a sustainability constraint is proposed that the different product models employ the containment relationship, which is a necessary condition for the subtractive remanufacturing. A novel level set-based product family representation is proposed to realize the containment relationship, and the related topology optimization problem is formulated and solved. In addition, spatial arrangement of the input design domains is explored to prevent highly stressed material regions from reusing. Feature-based level set concept for sustainability is then used. The novelty of the proposed method is that, for the first time, the product lifecycle issue of sustainability is addressed by a topology optimization method. The effectiveness of the proposed method is proved through a few numerical examples.
[DOI: 10.1115/1.4035052]

Keywords: level set, topology optimization, sustainability, remanufacturing

1 Introduction

In recent years, level set topology optimization (LSTO) has gained the popularity as a computational product design technique. It has demonstrated the adaptability subjected to different engineering disciplines. For instance, Wang et al. [1] and Allaire et al. [2] solved the compliance-minimization problems; and later, many other researchers investigated the stress-minimization and stress-constrained problems [3–8]; in Refs. [9–11], the multimaterial design problems were addressed. Other than the solid mechanics problems, LSTO has also been applied to design the fluid flow channels for energy dissipation minimization, and different flow types have been considered including Darcy flow, Stokes flow, and Navier–Stokes flow [12–15]; heat conduction problems were also addressed [16,17]. For more details, two comprehensive reviews can be found in Refs. [18,19].

As revealed by the literature survey that the authors conducted, so far, LSTO pursues the extreme structural performances; however, little attention was paid to other lifecycle aspects, including manufacture, operation/use, service/maintenance, and disposal/recycling [20]. It has always been a headache for engineers to manually post-treat the topology optimization solution to address these lifecycle considerations. Many researchers have realized this issue and several manufacture-oriented LSTO methods [21–24] have been developed to enhance the manufacturability. However, in general, many lifecycle aspects still lack solutions, which is also the case for other topology optimization methods [19].

Therefore, this paper presents a sustainable design-oriented LSTO method, which addresses the lifecycle issue of recycling. Sustainable design is popular and sometimes compulsive because it can reduce the negative environmental impact. An important strategy is to reuse the end-of-life (EoL) product, e.g., remanufacturing, and thus, to create a close-loop product lifecycle. Compared to the traditional landfilling, this strategy reduces the economic and environmental costs greatly. A few approaches of EoL product reuse are demonstrated in Fig. 1.

Among the approaches shown in Fig. 1, material recycling involves procedures of collecting, sorting, and processing the EoL product, through which raw materials are recycled and can be freely used in new production. However, both recycling and reproduction are energy-costly [25], and designers are reluctant to use the recycled materials because of the quality uncertainty [26].

Remanufacturing through additive manufacturing is an emerging and very promising approach, especially given the rapid development of additive manufacturing technology. This approach has been proven effective [27,28], which added new materials to an EoL product, either to repair the defects such as overwear, or to create new features to produce a different product model. However, there are limitations of this approach that the product quality processed through the currently available additive manufacturing methods is still unstable, e.g., property weakening [29], and very likely may not meet the expectations [30].

The third approach is to remanufacture the EoL product through the traditional subtractive machining. Product family is a widely accepted concept in industrial production, where a group of product models are produced through a common platform, and employ the similar function but different levels of performance. For instance, Fig. 2 shows a family of four-jaw support structures, each of which works under the same boundary condition, but demonstrates at a different level of load-bearing capacity. From the perspective of sustainability, it would be ideal that the high-level model coming to the EoL can be remanufactured through subtractive machining into another lower-level model (lower volume fraction). The overwear or corroded surfaces and the damaged areas could be removed to make it new. Advantages of this

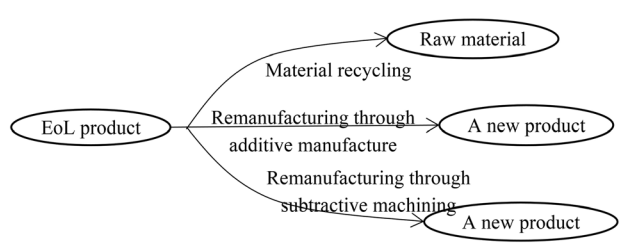

Fig. 1 Approaches of EoL product reuse

[1]Corresponding author.

Contributed by the Design Automation Committee of ASME for publication in the Journal of Mechanical Design. Manuscript received January 15, 2016; final manuscript received October 9, 2016; published online November 11, 2016. Assoc. Editor: James K. Guest.

 Copyright © 2017 by ASME

Downloaded From: http://mechanicaldesign.asmedigitalcollection.asme.org/ on 11/23/2016 Terms of Use: http://www.asme.org/about-asme/terms-of-use

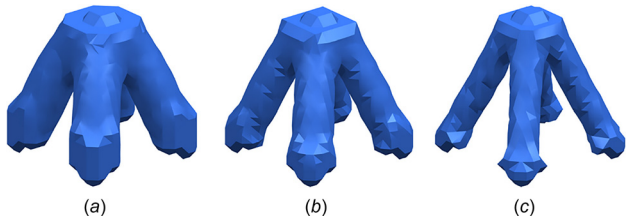

Fig. 2 Product family of the cube structure: (*a*) model 1 (volume ratio = 0.4), (*b*) model 2 (volume ratio = 0.3), and (*c*) model 3 (volume ratio = 0.2)

approach are evident that a remanufacturing process only consumes around 20–25% of the energy of the initial production [31], and it would not consume any energy to recycle the raw materials.

In summary, just as claimed in Ref. [25], remanufacturing through subtractive machining is the best among the three EoL product-reuse approaches simply because of the fact that, this approach is the most environmental-friendly and reliable for the current practice. To implement this approach, satisfying the containment relationship is mandatory, i.e., a product model should spatially be a subset of any higher-level model. This containment relationship is mathematically formulated in the following equation, which is named the sustainability constraint:

$$\Omega_i > \Omega_{i+1} \tag{1}$$

where Ω_i represents the material domain of model i, and the smaller number of i means a higher level.

Then, we explore the strategies of product family design through topology optimization. Figures 3(*a*) and 3(*b*) show two existing strategies. Subject to the compliance-minimization criteria, strategy 1 is simple and no adaption is required to the existing topology optimization algorithms. Specifically, the product family is composed of three models, which are sequentially designed through three mutually dependent topology optimization processes. That means the optimization result of model i is used as the input design domain of model $i+1$. With this strategy, the sustainability constraint is strictly satisfied. However, optimality of the low-level models is severely sacrificed because of the restricted design space. Strategy 2 is even simpler (see Fig. 3(*b*)), where all the topology optimization processes use the raw part as the input design domain and thus, all the models can be optimally designed given the fully explored design space. However, the sustainability constraints are very likely violated.

In this work, a novel strategy is proposed which concurrently addresses the overall design optimality and the sustainability constraints (Fig. 3(*c*)). To be specific, a level set-based product family representation is proposed which employs multiple level set functions to simultaneously represent the multiple product models. Accordingly, a multi-objective topology optimization problem is formulated through a weighted sum of structural performances of the multiple product models. During the solution process, the different product models are simultaneously optimized and interactively influenced to improve the overall optimality. A novel multilevel set interpolation is proposed to compulsively satisfy the sustainability constraints.

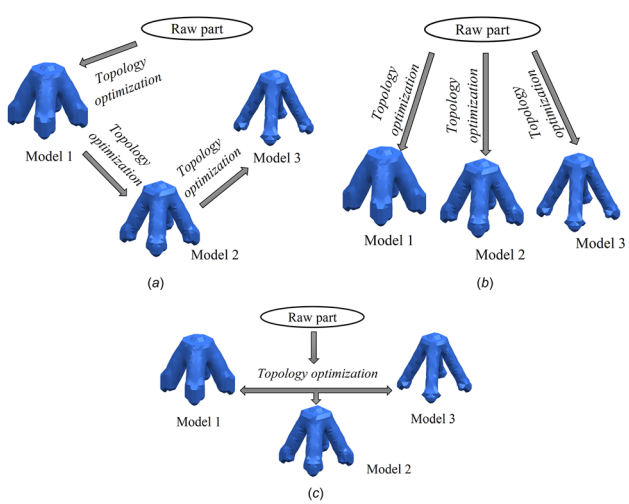

Fig. 3 Strategies of product family design: (*a*) strategy 1, (*b*) strategy 2, and (*c*) new strategy

Research innovation is evident that this is the first time the lifecycle issue of recycling is addressed by a topology optimization method. It is worth noticing that this method is much more complex than the product family design performed by Torstenfelt and Klarbring [32,33] which only realized the partial material domain overlap.

The following contents are organized as: Section 2 presents the conventional level set geometry modeling methods, including both the single-material and multimaterial schemes; Sec. 3 introduces the proposed level set-based product family representation, and the related topology optimization problem formulation; Sensitivity analysis is performed in Sec. 4; and two numerical examples are studied in Sec. 5; Sec. 6 explores design enhancement through spatial arrangement of the input design domains; Sec. 7 demonstrates the feature-based level set method for sustainability; A conclusion is given in Sec. 8.

2 Level Set Geometry Modeling

Osher and Sethian [34] proposed the level set function as a natural way of closed boundary representation. Specifically, let $D \in R^n$ $(n = 2 \text{ or } 3)$ be the initial design domain, $\Omega \in R^n$ $(n = 2 \text{ or } 3)$ represent the material domain, and $\partial\Omega$ be the material/void interface. The level set function, $\Phi(\mathbf{X}): R^n \mapsto R$, is defined as

$$\begin{cases} \Phi(\mathbf{X}) > 0, & \mathbf{X} \in \Omega/\partial\Omega \\ \Phi(\mathbf{X}) = 0, & \mathbf{X} \in \partial\Omega \\ \Phi(\mathbf{X}) < 0, & \mathbf{X} \in D/\Omega \end{cases} \tag{2}$$

Normally, the Heaviside function (see Eq. (3)) and the Dirac delta function (see Eq. (4)) are employed to support the numerical geometry modeling

$$\begin{cases} H(\Phi) = 1, & \Phi \geq 0 \\ H(\Phi) = 0, & \Phi < 0 \end{cases} \tag{3}$$

$$\delta(\Phi) = \partial H(\Phi)/\partial\Phi \tag{4}$$

Then, the interior and boundary of the material area can be represented by

$$\Omega = \{\mathbf{X} \mid H(\Phi(\mathbf{X})) = 1\} \tag{5}$$

$$\partial\Omega = \{\mathbf{X} \mid \delta(\Phi(\mathbf{X})) > 0\} \tag{6}$$

If applied to multimaterial geometry modeling, multiple level set functions are required. Generally, there are two approaches: the "color" level set [9] and the multimaterial level set (MMLS) [35]. Especially for the color level set, it has been widely accepted by multimaterial topology optimization implementations [9,10,36–38]. Other multimaterial level set models, such as piecewise constant level set [39–41] and reconciled level set [42], are also effective in supporting multimaterial topology optimization, which will not be specified in this paper.

The color level set approach was developed in Refs. [9,10], and it only requires m level set functions to represent $n = 2^m$ material phases. As presented in Fig. 4(*a*), the two level set functions $\Phi_i(\mathbf{X})$ $(i = 1, 2)$ could represent four material

Downloaded From: http://mechanicaldesign.asmedigitalcollection.asme.org/ on 11/23/2016 Terms of Use: http://www.asme.org/about-asme/terms-of-use

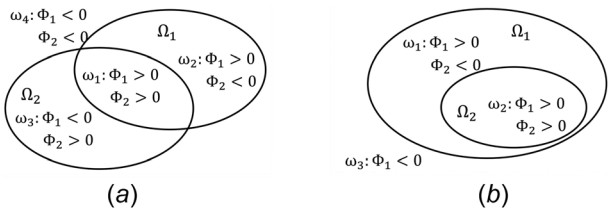

Fig. 4 Multimaterial level set geometry modeling

phases: $\omega_j = \{\mathbf{X} \mid \mathbf{H} = [H(\Phi_1(\mathbf{X})), H(\Phi_2(\mathbf{X}))] = \text{constant vector}\}$ $(j = 1,\ 2,\ 3,\ 4)$. The specific multimaterial interpolation is realized through the following equation:

$$\begin{aligned}\mathbf{D}(\mathbf{X}) = {} & H(\Phi_1(\mathbf{X}))H(\Phi_2(\mathbf{X}))\mathbf{D}^1 + H(\Phi_1(\mathbf{X}))[1 - H(\Phi_2(\mathbf{X}))]\mathbf{D}^2 \\ & + [1 - H(\Phi_1(\mathbf{X}))]H(\Phi_2(\mathbf{X}))\mathbf{D}^3 + [1 - H(\Phi_1(\mathbf{X}))] \\ & \times [1 - H(\Phi_2(\mathbf{X}))]\mathbf{D}^4\end{aligned} \tag{7}$$

in which $\mathbf{D}^1$, $\mathbf{D}^2$, $\mathbf{D}^3$, and $\mathbf{D}^4$ are the elasticity tensor of material phase 1, 2, 3, and 4, respectively.

The MMLS is a different approach that $m + 1$ material phases are represented by m level set functions. As presented in Fig. 4(*b*), the two level set functions $\Phi_i(\mathbf{X})$ $(i = 1,\ 2)$ represent three material phases: ω_j $(j = 1,\ 2,\ 3)$. Therefore, the multimaterial interpolation is formulated through

$$\begin{aligned}\mathbf{D}(\mathbf{X}) = {} & H(\Phi_1(\mathbf{X}))[1 - H(\Phi_2(\mathbf{X}))]\mathbf{D}^1 + H(\Phi_1(\mathbf{X}))H(\Phi_2(\mathbf{X}))\mathbf{D}^2 \\ & + [1 - H(\Phi_1(\mathbf{X}))]\mathbf{D}^3\end{aligned} \tag{8}$$

By using both approaches, the completeness $D = \cup_{k=1}^{n} \omega_k$ and uniqueness $\omega_k \cap \omega_l = \varnothing$ $(k \neq l)$ are satisfied.

3 Level Set-Based Product Family Modeling

Inspired by the MMLS, a novel approach is developed to support the product family modeling while satisfying the sustainability constraints.

As shown in Fig. 5, it requires m level set functions to represent m product models. The ith product model is defined by $\omega_i = \{\mathbf{X} | \Phi_1(\mathbf{X}) > 0, \ldots, \Phi_i(\mathbf{X}) > 0\}$. It is obvious that the sustainability constraints are compulsively satisfied. The related multilevel set interpolation would be

$$\begin{aligned}\mathbf{D}_1(\mathbf{X}) &= H(\Phi_1(\mathbf{X}))\overline{\mathbf{D}} \\ \mathbf{D}_2(\mathbf{X}) &= H(\Phi_1(\mathbf{X}))H(\Phi_2(\mathbf{X}))\overline{\mathbf{D}} \\ \mathbf{D}_3(\mathbf{X}) &= H(\Phi_1(\mathbf{X}))H(\Phi_2(\mathbf{X}))H(\Phi_3(\mathbf{X}))\overline{\mathbf{D}} \\ &\cdots\cdots\cdots\end{aligned} \tag{9}$$

where $\mathbf{D}_i(\mathbf{X})$ is the interpolated elasticity tensor of the product model i, and $\overline{\mathbf{D}}$ is the elasticity tensor of the solid material. It is

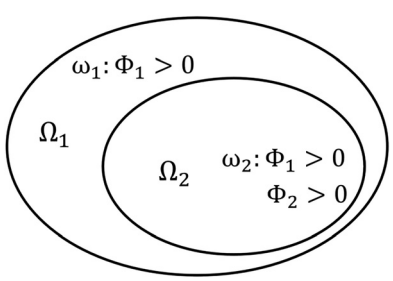

Fig. 5 Level set-based product family representation

noted that only one solid material type is involved because we assume the product to be homogeneous, which reflects the common case. The weak material properties for the void [1,2] are ignored in the expression but will be applied during numerical implementation. Accordingly, the compliance-minimization topology optimization problem for product family design is formulated as follows:

$$\begin{aligned}\text{Min.} \quad & J(\mathbf{u}_1, \mathbf{u}_2, \Phi_1, \Phi_2) \\ & = \mathbf{w}1\int_D \overline{\mathbf{D}}\mathbf{e}(\mathbf{u}_1)\mathbf{e}(\mathbf{u}_1)H(\Phi_1)d\Omega + \mathbf{w}2\int_D \overline{\mathbf{D}}\mathbf{e}(\mathbf{u}_2)\mathbf{e}(\mathbf{u}_2)H(\Phi_1) \\ & \qquad \times H(\Phi_2)d\Omega \\ \text{s.t.} \quad & a(\mathbf{u}_1, \mathbf{v}_1, \Phi_1) = l(\mathbf{v}_1) \\ & a(\mathbf{u}_2, \mathbf{v}_2, \Phi_1, \Phi_2) = l(\mathbf{v}_2) \quad \forall \mathbf{v}_1, \mathbf{v}_2 \in U_{ad} \\ & \int_D H(\Phi_1)d\Omega \leq V_1 \\ & \int_D H(\Phi_1)H(\Phi_2)d\Omega \leq V_2 \\ & a(\mathbf{u}_1, \mathbf{v}_1, \Phi_1) = \int_D \overline{\mathbf{D}}\mathbf{e}(\mathbf{u}_1)\mathbf{e}(\mathbf{v}_1)H(\Phi_1)d\Omega \\ & a(\mathbf{u}_2, \mathbf{v}_2, \Phi_1, \Phi_2) = \int_D \overline{\mathbf{D}}\mathbf{e}(\mathbf{u}_2)\mathbf{e}(\mathbf{v}_2)H(\Phi_1)H(\Phi_2)d\Omega \\ & l(\mathbf{v}_1) = \int_D \mathbf{p}\mathbf{v}_1 d\Omega + \int_D \boldsymbol{\tau}\mathbf{v}_1 dS \\ & l(\mathbf{v}_2) = \int_D \mathbf{p}\mathbf{v}_2 d\Omega + \int_D \boldsymbol{\tau}\mathbf{v}_2 dS\end{aligned} \tag{10}$$

in which $a()$ is the energy bilinear form and $l()$ is the load linear form. $\mathbf{u}$ is the deformation vector, $\mathbf{v}$ is the test vector, and $\mathbf{e}(\mathbf{u})$ is the strain. $U = \{\mathbf{v} \in H^1(\Omega)^d | \mathbf{v} = 0 \text{ on } \Gamma_D\}$ is the space of kinematically admissible displacement field, $\mathbf{p}$ is the body force, and $\boldsymbol{\tau}$ is the boundary traction force, which are assumed not spatially varying. V_1 and V_2 are the upper bounds of the material volume for product model 1 and 2, respectively. $\mathbf{w}1$ and $\mathbf{w}2$ are the weighting factors, which satisfy $\mathbf{w}1 + \mathbf{w}2 = 1$.

It is noted that this problem formulation is defined by assuming only two product models and it would be trivial to make the extensions.

We can see from Eq. (10) that this is a multi-objective optimization problem and the objective function is a weighted sum of the structural compliances of the two product models. Two finite element analyses are required in each iteration to separately evaluate the status variables $\mathbf{u}_1$ and $\mathbf{u}_2$.

4 Sensitivity Analysis

In order to solve the optimization problem, the level set functions Φ_1 and Φ_2 are used as design variables. The sensitivity analysis is needed to derive the velocity fields V_{n1} and V_{n2} to properly evolve the level set contours in the steepest descent direction. Generally, the Lagrange multiplier method is applied to solve the optimization problem; material derivative and the adjoint method are employed for shape sensitivity analysis. The shape sensitivity analysis for multimaterial compliance-minimization problem under the level set framework is well known, which have been presented in previous publications [35,37]. Therefore, the detailed process will not be repeated while only the major results are presented; see below

$$\begin{aligned}L' &= \int_D R_1\delta(\Phi_1)V_{n1}|\nabla\Phi_1|d\Omega + \int_D R_2\delta(\Phi_2)V_{n2}|\nabla\Phi_2|d\Omega \\ R_1 &= \lambda_1 + \lambda_2 H(\Phi_2) - \mathbf{w}1 \times \overline{\mathbf{D}}\mathbf{e}(\mathbf{u}_1)\mathbf{e}(\mathbf{u}_1) - \mathbf{w}2 \times \overline{\mathbf{D}}\mathbf{e}(\mathbf{u}_2)\mathbf{e}(\mathbf{u}_2) \\ & \qquad \times H(\Phi_2) \\ R_2 &= \lambda_2 H(\Phi_1) - \mathbf{w}2 \times \overline{\mathbf{D}}\mathbf{e}(\mathbf{u}_2)\mathbf{e}(\mathbf{u}_2)H(\Phi_1)\end{aligned} \tag{11}$$

Downloaded From: http://mechanicaldesign.asmedigitalcollection.asme.org/ on 11/23/2016 Terms of Use: http://www.asme.org/about-asme/terms-of-use

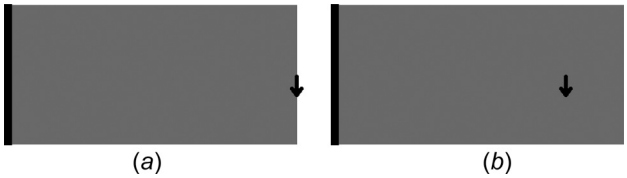

Fig. 6 Boundary conditions of (*a*) model 1 and (*b*) model 2

where L is the Lagrangian; λ_1 and λ_2 are the Lagrange multipliers; R_1 and R_2 are the shape sensitivity densities.

Then, by following equation:

$$\begin{aligned} V_{n1} &= -R_1 \\ V_{n2} &= -R_2 \end{aligned} \tag{12}$$

L can be guaranteed to change in the descent direction, as shown in the following equation:

$$L' = \int_D -R_1^2 \delta(\Phi_1)|\nabla\Phi_1| d\Omega + \int_D -R_2^2 \delta(\Phi_2)|\nabla\Phi_2| d\Omega \tag{13}$$

Guided by the calculated velocity fields, update of the level set contours can be performed by solving the Hamilton–Jacobi equation. This is well established and details will not be repeated here. Interested readers can refer to Refs. [1,2].

5 Numerical Example

In this section, the benchmark cantilever example is studied to prove the effectiveness of the proposed method. We assume that two models form the product family and the related boundary conditions are presented in Fig. 6. The same homogeneous elastic material is applied to both models which employs the Young's modulus of 1.3 and the Poisson's ratio of 0.4. The optimization problem is to minimize the structural compliance under the maximum volume fraction of 0.5 for model 1 and 0.4 for model 2.

The solution of only running model 1 is demonstrated in Fig. 7. It is observed that the loading point of model 2 is in status of void, which means the sequential procedure, as shown in Fig. 3(*a*), cannot be applied. Therefore, among the three strategies as presented in Fig. 3, the newly proposed strategy is appropriate to solve this sustainability-constrained problem.

To demonstrate the effectiveness of the proposed method, a few numerical implementations are performed under different weight factors. The optimization results are presented in Fig. 8.

Through analysis of the optimization results, it can be concluded that the proposed method can effectively design the product family, and the sustainability constraints are always satisfied. In addition, as indicated by Fig. 9, result optimality of the two models is balanced by the weight factor.

In Fig. 8, the derived structural topologies of the different product models are always identical, while it should not be the case if the volume fraction difference is enlarged. Therefore, this example is further studied subjected to maximum material fraction of 0.5 for model 1 and 0.25 for model 2. The related optimization results are demonstrated in Fig. 10. We can see from the results that, by increasing the volume fraction difference, the derived structural topologies are not always consistent.

Fig. 7 The independent solution of model 1

6 Spatial Arrangement of the Design Domains

In Sec. 5, spatial arrangement of the input design domains is randomly determined and thus, there is still room to further enhance the overall design effect by carefully exploring the spatial arrangement. Principally, it is preferable to prevent the highly stressed material regions from reusing. In addition, the derived structural performances are tightly related to the spatial arrangement and it is of our interest to investigate how the structural performances will be affected.

6.1 The Cantilever Structure Problem. For the cantilever structure, material areas around the left edge are highly stressed. Therefore, it is preferable to remove these areas when reusing the part, which can be achieved by repositioning the boundary condition of model 2; see Fig. 11.

Correspondingly, the optimization results are demonstrated in Fig. 12. It can be foreseen that the results of model 2 after spatial arrangement are more reliable because the reused materials are less stressed in history.

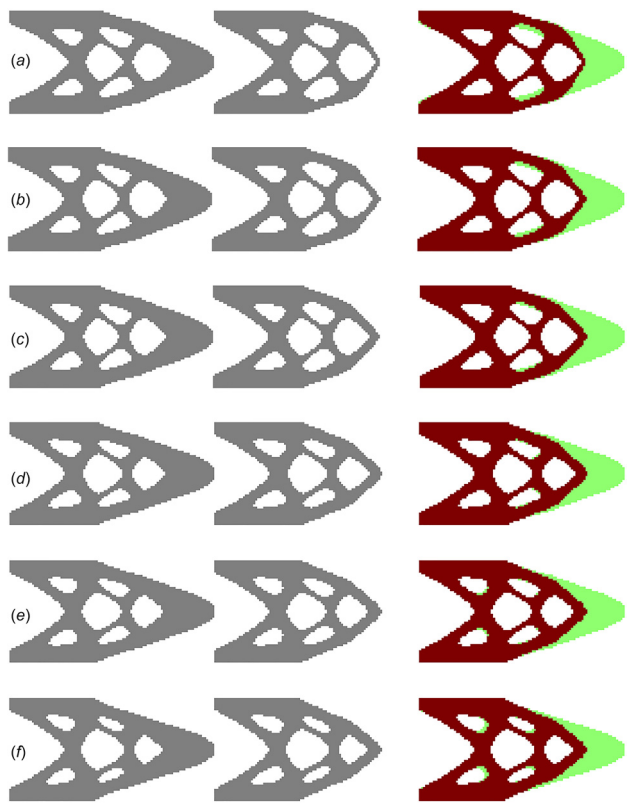

Fig. 8 Optimization results under different weight factors. (*a*) Results of model 1 (compliance = 51.68), model 2 (compliance = 34.52), and the spatial overlap under the weight factor w1 = 0.9; (*b*) results of model 1 (compliance = 51.99), model 2 (compliance = 32.42), and the spatial overlap under the weight factor w1 = 0.8; (*c*) results of model 1 (compliance = 52.09), model 2 (compliance = 32.08), and the spatial overlap under the weight factor w1 = 0.7; (*d*) results of model 1 (compliance = 53.40), model 2 (compliance = 30.81), and the spatial overlap under the weight factor w1 = 0.6; (*e*) results of model 1 (compliance = 54.76), model 2 (compliance = 30.90), and the spatial overlap under the weight factor w1 = 0.5; and (*f*) results of model 1 (compliance = 56.21), model 2 (compliance = 30.70), and the spatial overlap under the weight factor w1 = 0.4.

Downloaded From: http://mechanicaldesign.asmedigitalcollection.asme.org/ on 11/23/2016 Terms of Use: http://www.asme.org/about-asme/terms-of-use

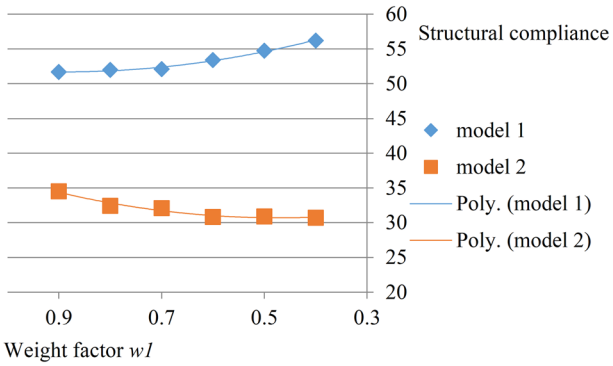

Fig. 9 Influence of the weight factor

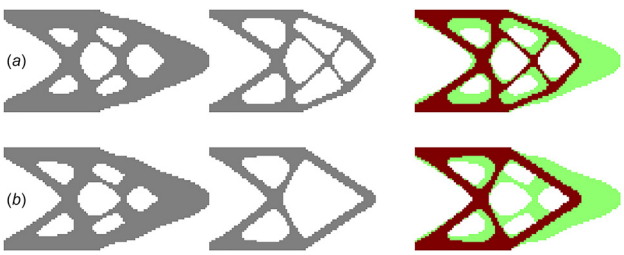

Fig. 10 Optimization results after changing the volume fractions: (*a*) results of model 1 (compliance = 52.66), model 2 (compliance = 49.41), and the spatial overlap under the weight factor w1 = 0.8; (*b*) results of model 1 (compliance = 54.99), model 2 (compliance = 47.18), and the spatial overlap under the weight factor w1 = 0.4

6.2 The L-Bracket Problem. In this example, the same homogeneous elastic material is applied to both models which employs the Young's modulus of 1.3 and the Poisson's ratio of 0.4. The optimization problem is to minimize the structural compliance under the maximum material volume fraction of 0.4 for model 1 and 0.2 for model 2.

The boundary condition of model 1 is shown in Fig. 13(*a*) and two sets of boundary conditions are applied to model 2; see Figs. 13(*b*) and 13(*c*), which correspond to the two sets of spatial arrangements.

The optimization results are presented in Fig. 14 given the spatial arrangement 1 and in Fig. 15 given the spatial arrangement 2.

Generally, the most stressed area of the L-bracket locates at the reentrant corner. Therefore, it is observed from Figs. 14 and 15 that the optimization results subjected to the spatial arrangement 2 effectively prevent most of the highly stressed areas from reusing. In addition, the derived structural performances subjected to the spatial arrangement 2 are obviously better than those of the spatial arrangement 1.

7 Feature-Based Product Family Design

Geometric features are widely applied in mechanical engineering domain, especially for design and manufacturing activities. Therefore, this section presents the feature-based level set method subjected to the sustainability consideration.

Fig. 11 Rearrangement of the boundary condition of model 2

7.1 Feature-Based Level Set Geometry Modeling. First, individual geometric features can be represented by parametric level set functions. For instance, a circle feature can be modeled by

$$\Phi_f(\mathbf{X}) = R_c - \mathrm{sqrt}((x - x_0)^2 + (y - y_0)^2) \tag{14}$$

and a square feature by

$$\Phi_f(\mathbf{X}) = \min\left\{\frac{H_s}{2} - (x - x_0),\ \frac{H_s}{2} + (x - x_0), \frac{H_s}{2} - (y - y_0),\ \frac{H_s}{2} + (y - y_0)\right\} \tag{15}$$

in which (x_0, y_0) is the feature primitive center coordinates; R_c is the circle radius; and H_s is the square length.

Then, a complex geometry can be constructed through Boolean operations of the individual feature primitives; see the following equation for the Boolean operators:

$$\begin{aligned} \Phi_{f1} \cup \Phi_{f2} &= \max(\Phi_{f1},\ \Phi_{f2}) \\ \Phi_{f1} \cap \Phi_{f2} &= \min(\Phi_{f1},\ \Phi_{f2}) \\ \Phi_{f1} \backslash \Phi_{f2} &= \min(\Phi_{f1}, -\Phi_{f2}) \end{aligned} \tag{16}$$

Finally, the geometry is constructed through the following equation:

$$\Phi(\mathbf{X}) = C(\Phi_{f1}, \Phi_{f2}, \Phi_{f3}, \ldots) \tag{17}$$

where C is the set of Boolean operations. It is worth noting that, level set topology optimization on constructive solid geometry (CSG) model was originally studied in Ref. [43]. About Eqs. (15)–(17), they are C1 discontinuous, which are nondifferentiable. This issue can be solved by employing differentiable geometry representations by smoothing the sharp corners [44–46] and the analytical descriptions of the Boolean operators [47]. On the other hand, in many topology optimization implementations involving discrete geometric elements, Eqs. (15)–(17) are directly applied to calculate the piecewise continuous sensitivity result, which has been proven effective by many numerical implementations [44,45,47].

7.2 A Torque Arm Example. As depicted in Figs. 16(*a*) and 16(*b*), the two torque arm product models are both geometric feature based, and the common hierarchical structure of Boolean operations is demonstrated in Fig. 16(*c*) and in the following equation:

$$\begin{aligned} \Phi_1 &= (\Phi_{f1} \cup \Phi_{f2} \cup \Phi_{f3})/(\Phi_{f4} \cup \Phi_{f5} \cup \Phi_{f6}) \quad \text{(model 1)} \\ \Phi_2 &= (\Phi_{F1} \cup \Phi_{F2} \cup \Phi_{F3})/(\Phi_{F4} \cup \Phi_{F5} \cup \Phi_{F6}) \quad \text{(model 2)} \end{aligned} \tag{18}$$

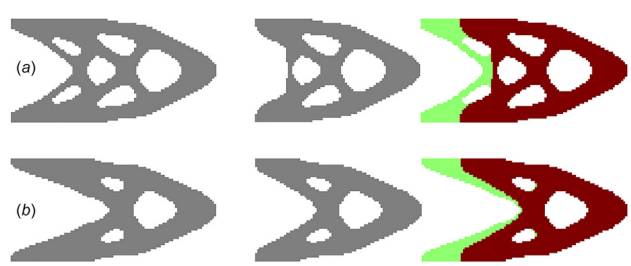

Fig. 12 Optimization results after spatial arrangement: (*a*) results of model 1 (compliance = 51.88), model 2 (compliance = 31.74), and the spatial overlap under the weight factor w1 = 0.5; (*b*) results of model 1 (compliance = 56.44), model 2 (compliance = 30.83), and the spatial overlap under the weight factor w1 = 0.2

Downloaded From: http://mechanicaldesign.asmedigitalcollection.asme.org/ on 11/23/2016 Terms of Use: http://www.asme.org/about-asme/terms-of-use

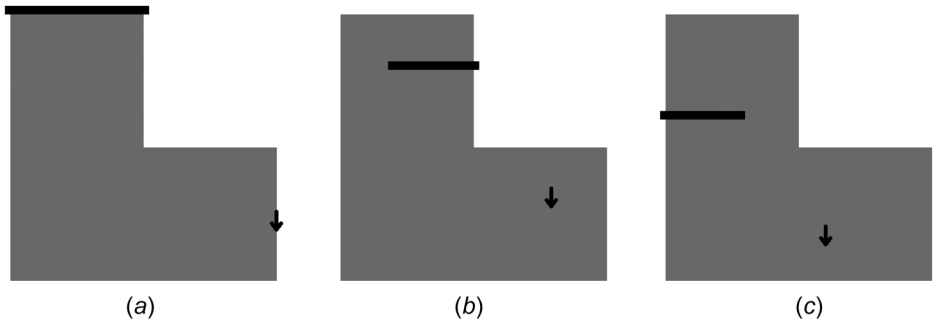

Fig. 13 Boundary conditions of (*a*) model 1, (*b*) model 2 (given the spatial arrangement 1), and (*c*) model 2 (given the spatial arrangement 2)

We can see that the initial design domains are not identical. Therefore, a preparation step is necessary to unify the separated design domains by overlapping the fixed circular voids, and the unified design domain is represented by Eq. (19).

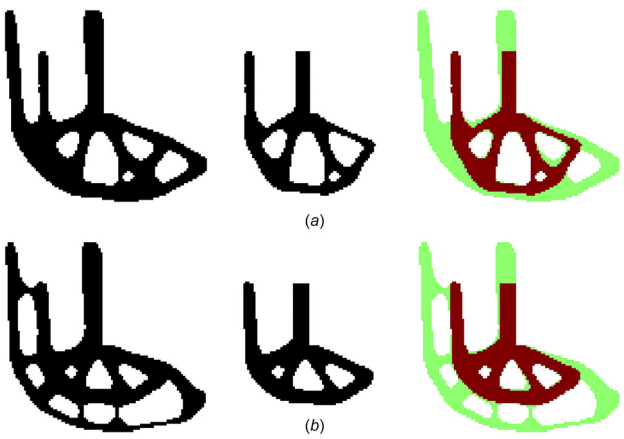

Fig. 14 Optimization results subject to the spatial arrangement 1: (*a*) results of model 1 (compliance = 80.51), model 2 (compliance = 53.57), and the spatial overlap under the weight factor w1 = 0.5; (*b*) results of model 1 (compliance = 89.90), model 2 (compliance = 50.03), and the spatial overlap under the weight factor w1 = 0.2

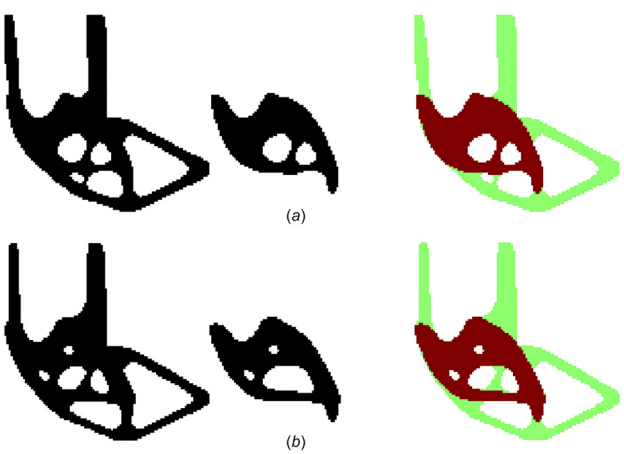

Fig. 15 Optimization results subject to the spatial arrangement 2: (*a*) results of model 1 (compliance = 77.39), model 2 (compliance = 20.27), and the spatial overlap under the weight factor w1 = 0.5; (*b*) results of model 1 (compliance = 84.67), model 2 (compliance = 18.93), and the spatial overlap under the weight factor w1 = 0.2

$$\Phi = \Phi_1 \cup \Phi_2 \tag{19}$$

The next step is to distinguish the design domain into designable and nondesignable subdomains because some geometric features are employed for assembly purpose and therefore, their shape characteristics should be resevered. Hence, in this example, Φ_{f1} (Φ_{F1}), Φ_{f3} (Φ_{F3}), Φ_{f4} (Φ_{F4}), and Φ_{f6} (Φ_{F6}) are nondesignable, while only Φ_{f2} (Φ_{F2}) and Φ_{f5} (Φ_{F5}) are freely designable subdomains.

Equation (10) is still applied as the optimization problem formulation. The maximum material volume fraction is 0.4 for model 1 and 0.3 for model 2. Again, a few numerical implementations are conducted under different weight factors, and the optimization results are shown in Fig. 17.

Through analysis, similar conclusions can be drawn regarding the cantilever example: the sustainability constraints are always satisfied and the weight factor can well balance the design quality between the two models; see Fig. 18.

8 Conclusion

This paper contributes toward a novel sustainable design-oriented LSTO method. It addresses the sustainability issue of product family design, for the first time, through topology optimization. The proposed method enables EoL product reuse; this

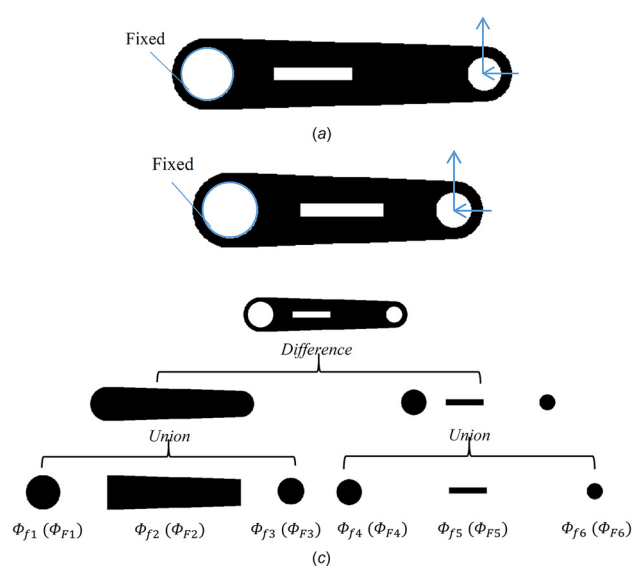

Fig. 16 The torque arm example: (*a*) the design domain and boundary condition of model 1; (*b*) the design domain and boundary condition of model 2; and (*c*) construction of the geometry through *R*-functions

Downloaded From: http://mechanicaldesign.asmedigitalcollection.asme.org/ on 11/23/2016 Terms of Use: http://www.asme.org/about-asme/terms-of-use

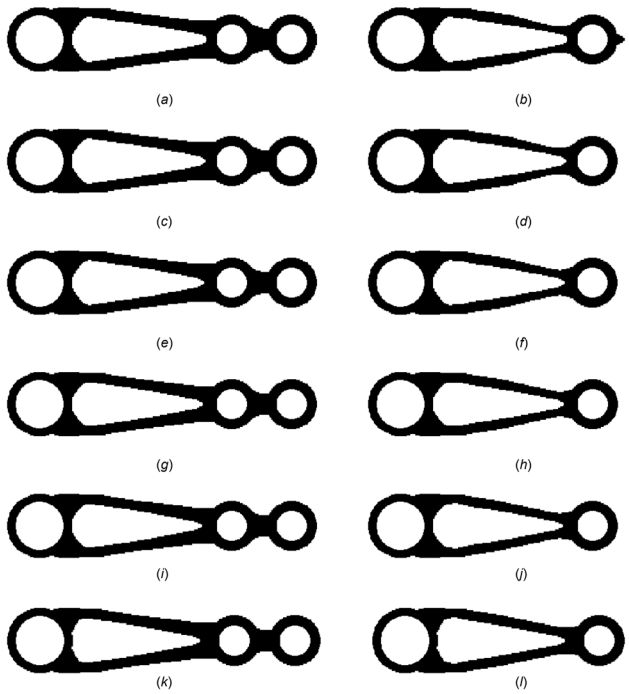

Fig. 17 Optimization results under different weight factors: (*a*) model 1 (w1 = 0.9), (*b*) model 2 (w1 = 0.9), (*c*) model 1 (w1 = 0.8), (*d*) model 2 (w1 = 0.8), (*e*) model 1 (w1 = 0.7), (*f*) model 2 (w1 = 0.7), (*g*) model 1 (w1 = 0.6), (*h*) model 2 (w1 = 0.6), (*i*) model 1 (w1 = 0.5), (*j*) model 2 (w1 = 0.5), (*k*) model 1 (w1 = 0.4), and (*l*) model 2 (w1 = 0.4)

function is of engineering significance to reduce production-related environmental and energy issues through remanufacturing.

Technically, a sustainability constraint is proposed that the different product models employ the containment relationship. This sustainability constraint is addressed through a novel multilevel set interpolation, which is inspired by the previous MMLS modeling. The overall design optimality is guaranteed by the concurrent multiproduct model optimization.

Spatial arrangement of the input design domains is explored to prevent highly stressed material regions from reusing because these regions are prone to accumulating fatigue damages. Through two numerical studies, it is proven that the highly stressed areas can be prevented from reusing through spatial arrangement, and the rearranged design domains do not evidently sacrifice the derived structural performances. Hence, carefully positioning the input design domains is an effective approach to enhancing reusability of the product models.

On the other hand, a more stringent way to consider the fatigue damage is to add local fatigue constraints when formulating the optimization problem [48]. However, fatigue-constrained topology optimization falls out of scope of this paper, and the main focus, as well as the contribution, of this paper is the sustainability-oriented product family design method through a novel multilevel set interpolation. It is practically meaningful because load-bearing parts come to EoL for many possible reasons, e.g., overwear and corrosion, instead of only fatigue damage or direct failure. Even so, it is of the authors' interest to explore the fatigue-constrained product family design in our future work.

At the end, a few limitations of this work are stated here: (i) subtractive machining constraints are not included in the proposed topology optimization method, such as tool access, which causes that the optimized topology design may face challenges for manufacturing; and (ii) so far, the proposed method is limited to compliance minimization, which is monotonic with volume. For other highly relevant design criteria, such as stresses, the applicability of the proposed method needs more research effort and enhancement. Hence, overcoming these limitations will be the main focus of our future work.

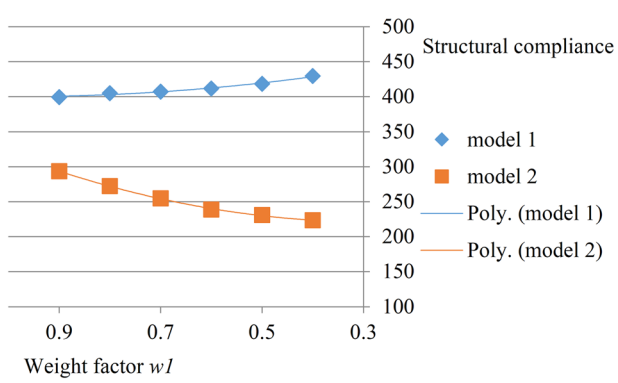

Fig. 18 Influence of the weight factor

Acknowledgment

The authors would like to acknowledge the support from China Scholarship Council (CSC) and Natural Sciences and Engineering Research Council of Canada (NSERC).

References

[1] Wang, M. Y., Wang, X. M., and Guo, D. M., 2003, "A Level Set Method for Structural Topology Optimization," Comput. Methods Appl. Mech. Eng., **192**, pp. 227–246.
[2] Allaire, G., Jouve, F., and Toader, A. M., 2004, "Structural Optimization Using Sensitivity Analysis and a Level-Set Method," J. Comput. Phys., **104**, pp. 363–393.
[3] Allaire, G., and Jouve, F., 2008, "Minimum Stress Optimal Design With the Level Set Method," Eng. Anal. Boundary Elem., **32**(11), pp. 909–918.
[4] Guo, X., Zhang, W. S., Wang, M. Y., and Wei, P., 2011, "Stress-Related Topology Optimization Via Level Set Approach," Comput. Methods Appl. Mech. Eng., **200**, pp. 3439–3452.
[5] Xia, Q., Shi, T. L., Liu, S. Y., and Wang, M. Y., 2012, "A Level Set Solution to the Stress-Based Structural Shape and Topology Optimization," Comput. Struct., **90–91**, pp. 55–64.
[6] Wang, M. Y., and Li, L., 2013, "Shape Equilibrium Constraint: A Strategy for Stress-Constrained Structural Topology Optimization," Struct. Multidisc. Optim., **47**(3), pp. 335–352.
[7] Zhang, W. S., Guo, X., Wang, M. Y., and Wei, P., 2013, "Optimal Topology Design of Continuum Structures With Stress Concentration Alleviation Via Level Set Method," Int. J. Numer. Methods Eng., **93**(9), pp. 942–959.
[8] Emmendoerfer, H., Jr., and Fancello, E. A., 2014, "A Level Set Approach for Topology Optimization With Local Stress Constraints," Int. J. Numer. Methods Eng., **99**(2), pp. 129–156.
[9] Wang, M. Y., and Wang, X. M., 2004, "Color Level Sets: A Multi-Phase Method for Structural Topology Optimization With Multiple Materials," Comput. Methods Appl. Mech. Eng., **193**, pp. 469–496.
[10] Wang, M. Y., and Wang, X. M., 2005, "A Level-Set Based Variational Method for Design and Optimization of Heterogeneous Objects," Comput. Aided Des., **37**(3), pp. 321–337.
[11] Xia, Q., and Wang, M. Y., 2008, "Simultaneous Optimization of the Material Properties and the Topology of Functionally Graded Structures," Comput. Aided Des., **40**(6), pp. 660–675.
[12] Zhou, S. W., and Li, Q., 2008, "A Variational Level Set Method for the Topology Optimization of Steady-State Navier–Stokes Flow," J. Comput. Phys., **227**(24), pp. 10178–10195.
[13] Challis, V. J., and Guest, J. K., 2009, "Level Set Topology Optimization of Fluids in Stokes Flow," Int. J. Numer. Methods Eng., **79**(10), pp. 1284–1308.
[14] Deng, Y. B., Zhang, P., Liu, Y. S., Wu, Y. H., and Liu, Z. Y., 2013, "Optimization of Unsteady Incompressible Navier–Stokes Flows Using Variational Level Set Method," Int. J. Numer. Methods Eng., **71**(12), pp. 1475–1493.
[15] Deng, Y. B., Liu, Z. Y., Wu, J. F., and Wu, Y. H., 2013, "Topology Optimization of Steady Navier–Stokes Flow With Body Force," Comput. Methods Appl. Mech. Eng., **255**, pp. 306–321.
[16] Ha, S. H., and Cho, S., 2005, "Topological Shape Optimization of Heat Conduction Problems Using Level Set Approach," Numer. Heat Transfer, Part B, **48**(1), pp. 67–88.
[17] Zhuang, C. G., Xiong, Z. H., and Ding, H., 2007, "A Level Set Method for Topology Optimization of Heat Conduction Problem Under Multiple Load Cases," Comput. Methods Appl. Mech. Eng., **196**, pp. 1074–1084.
[18] van Dijk, N. P., Maute, K., Langelaar, M., and van Keulen, F., 2013, "Level-Set Methods for Structural Topology Optimization: A Review," Struct. Multidisc. Optim., **48**(3), pp. 437–472.

Downloaded From: http://mechanicaldesign.asmedigitalcollection.asme.org/ on 11/23/2016 Terms of Use: http://www.asme.org/about-asme/terms-of-use

[19] Sigmund, O., and Maute, K., 2013, "Topology Optimization Approaches," Struct. Multidisc. Optim., **48**(6), pp. 1031–1055.
[20] Lee, S. G., Ma, Y. S., Thimm, G. L., and Verstraeten, J., 2008, "Product Lifecycle Management in Aviation Maintenance, Repair and Overhaul," Comput. Ind., **59**, pp. 296–303.
[21] Xia, Q., Shi, T. L., Wang, M. Y., and Liu, S. Y., 2010, "A Level Set Based Method for the Optimization of Cast Part," Struct. Multidisc. Optim., **41**(5), pp. 735–747.
[22] Allaire, G., Jouve, F., and Michailidis, G., 2013, "Casting Constraints in Structural Optimization Via a Level-Set Method," 10th World Congress on Structural and Multidisciplinary Optimization, Orlando, FL, May.
[23] Liu, J. K., Ma, Y. S., Fu, J. Y., and Duke, K., 2015, "A Novel CACD/CAD/CAE Integrated Design Framework for Fiber-Reinforced Plastic Parts," Adv. Eng. Software, **87**, pp. 13–29.
[24] Liu, J. K., and Ma, Y. S., 2015, "3D Level-Set Topology Optimization: A Machining Feature-Based Approach," Struct. Multidisc. Optim., **52**(3), pp. 563–582.
[25] King, A. M., Burgess, S. C., Ijomah, W., and McMahon, C. A., 2006, "Reducing Waste: Repair, Recondition, Remanufacture or Recycle?," Sustainable Dev., **14**(4), pp. 257–267.
[26] Chick, A., and Micklethwaite, P., 2002, "Obstacles to UK Architects and Designers Specifying Recycled Products and Materials," Design History Society Conference, Aberystwyth, UK, Sept. 3–5.
[27] Le, V. T., Paris, H., and Mandil, G., 2015, "Using Additive and Subtractive Manufacturing Technologies in a New Remanufacturing Strategy to Produce New Parts From End-of-Life Parts," 22nd France Mechanical Congress, Lyon, France, Aug. 24–28.
[28] Mandil, G., Le, V. T., Paris, H., and Suard, M., 2016, "Building New Entities From Existing Titanium Part by Electron Beam Melting: Microstructures and Mechanical Properties," Int. J. Adv. Manuf. Technol., **85**(5), pp. 1835–1846.
[29] Ulu, E., Korkmaz, E., Yay, K., Ozdoganlar, O. B., and Kara, L. B., 2015, "Enhancing the Structural Performance of Additively Manufactured Objects Through Build Orientation Optimization," ASME J. Mech. Des., **137**(11), p. 111410.
[30] Frazier, W. E., 2014, "Metal Additive Manufacturing: A Review," J. Mater. Eng. Perform., **23**(6), pp. 1917–1928.
[31] Lund, R., 1985, "Remanufacturing: The Experience of the United States and Implications for Developing Countries," The World Bank, Washington, DC, Technical Paper No. 31, UNDP Project Management Report 2.
[32] Torstenfelt, B., and Klarbring, A., 2006, "Structural Optimization of Modular Product Families With Application to Car Space Frame Structures," Struct. Multidisc. Optim., **32**(2), pp. 133–140.
[33] Torstenfelt, B., and Klarbring, A., 2007, "Conceptual Optimal Design of Modular Car Product Families Using Simultaneous Size, Shape and Topology Optimization," Finite Elem. Anal. Des., **43**(14), pp. 1050–1061.
[34] Osher, S., and Sethian, J. A., 1988, "Front Propagating With Curvature-Dependent Speed: Algorithms Based on Hamilton–Jacobi Formulations," J. Comput. Phys., **79**(1), pp. 12–49.
[35] Wang, Y. Q., Luo, Z., Kang, Z., and Zhang, N., 2015, "A Multi-Material Level Set-Based Topology and Shape Optimization Method," Comput. Methods Appl. Mech. Eng., **283**, pp. 1570–1586.
[36] Wang, M. Y., Chen, S. K., Wang, X., and Mei, Y., 2005, "Design of Multi-Material Compliant Mechanism Using Level Set Methods," ASME J. Mech. Des., **127**(5), pp. 941–956.
[37] Guo, X., Zhang, W. S., and Zhong, W. L., 2014, "Stress-Related Topology Optimization of Continuum Structures Involving Multi-Phase Materials," Comput. Methods Appl. Mech. Eng., **268**, pp. 632–655.
[38] Michailidis, G., 2014, "Manufacturing Constraints and Multi-Phase Shape and Topology Optimization Via a Level-Set Method," Doctoral dissertation, Ecole Polytechnique X, Palaiseau, France.
[39] Li, H. W., and Tai, X. C., 2006, "Piecewise Constant Level Set Methods for Multiphase Motion," University of California at Los Angeles, Los Angeles, CA, Technical Report No. 06-17.
[40] Wei, P., and Wang, M. Y., 2009, "Piecewise Constant Level Set Method for Structural Topology Optimization," Int. J. Numer. Methods Eng., **78**(4), pp. 379–402.
[41] Luo, Z., Tong, L., Luo, J., Wei, P., and Wang, M. Y., 2009, "Design of Piezoelectric Actuators Using a Multiphase Level Set Method of Piecewise Constants," J. Comput. Phys., **228**(7), pp. 2643–2659.
[42] Chen, S., Gonella, S., Chen, W., and Liu, W. K., 2010, "A Level Set Approach for Optimal Design of Smart Energy Harvesters," Comput. Methods Appl. Mech. Eng., **199**, pp. 2532–2543.
[43] Chen, J., Shapiro, V., Suresh, K., and Tsukanov, I., 2007, "Shape Optimization With Topological Changes and Parametric Control," Int. J. Numer. Methods Eng., **71**(3), pp. 313–346.
[44] Guo, X., Zhang, W. S., and Zhong, W. L., 2014, "Doing Topology Optimization Explicitly and Geometrically—A New Moving Morphable Components Based Framework," ASME J. Appl. Mech., **81**(8), p. 081009.
[45] Zhang, W. S., Yuan, J., Zhang, J., and Guo, X., 2016, "A New Topology Optimization Approach Based on Moving Morphable Components (MMC) and the Ersatz Material Model," Struct. Multidisc. Optim., **53**(6), pp. 1243–1260.
[46] Norato, J. A., Bell, B. K., and Tortorelli, D. A., 2015, "A Geometry Projection Method for Continuum-Based Topology Optimization With Discrete Elements," Comput. Methods Appl. Mech. Eng., **293**, pp. 306–327.
[47] Mei, Y. L., Wang, X. M., and Cheng, G. D., 2008, "A Feature-Based Topological Optimization for Structure Design," Adv. Eng. Software, **39**(2), pp. 71–87.
[48] Holmberg, E., Torstenfelt, B., and Klarbring, A., 2014, "Fatigue Constrained Topology Optimization," Struct. Multidisc. Optim., **50**(2), pp. 207–219.

Downloaded From: http://mechanicaldesign.asmedigitalcollection.asme.org/ on 11/23/2016 Terms of Use: http://www.asme.org/about-asme/terms-of-use